Published in final edited form as:
Cell Rep. 2014 September 25; 8(6): 1819–1831. doi:10.1016/j.celrep.2014.08.036.

ARTD1/PARP1 negatively regulates glycolysis by inhibiting hexokinase 1 independent of NAD+ depletion

Elise Fouquerel[1,2,†], **Eva M. Goellner**[1,2,+,†], **Zhongxun Yu**[2,3], **Jean-Philippe Gagné**[4], **Michelle Barbi de Moura**[1,2], **Tim Feinstein**[1], **David Wheeler**[1], **Philip Redpath**[5], **Jianfeng Li**[1,2], **Guillermo Romero**[1], **Marie Migaud**[5], **Bennett Van Houten**[1,2], **Guy G. Poirier**[4], and **Robert W. Sobol**[1,2,6,*]

[1]Department of Pharmacology & Chemical Biology, University of Pittsburgh School of Medicine, Pittsburgh, PA 15213, USA

[2]University of Pittsburgh Cancer Institute, Hillman Cancer Center, Pittsburgh, PA 15213, USA

[3]School of Medicine, Tsinghua University, No.1 Tsinghua Yuan, Haidian District, Beijing 100084, China

[4]Centre de recherche du CHU de Québec, Université Laval, Faculté de Médecine, Québec, Canada.

[5]School of Pharmacy, Queen's University, Belfast, BT9 7BL, UK

[6]Department of Human Genetics, University of Pittsburgh Graduate School of Public Health, Pittsburgh, PA, 15213, USA

Summary

ARTD1 (PARP1) is a key enzyme involved in DNA repair by synthesizing poly(ADP-ribose) (PAR) in response to strand breaks and plays an important role in cell death following excessive DNA damage. ARTD1-induced cell death is associated with NAD^+ depletion and ATP loss, however the molecular mechanism of ARTD1-mediated energy collapse remains elusive. Using real-time metabolic measurements, we directly compared the effects of ARTD1 activation and direct NAD^+ depletion. We found that ARTD1-mediated PAR synthesis, but not direct NAD^+ depletion, resulted in a block to glycolysis and ATP loss. We then established a proteomics based

*Correspondence: Robert W. Sobol, PhD, Hillman Cancer Center, University of Pittsburgh Cancer Institute Research Pavilion, Suite 2.6a, 5117 Centre Avenue; Pittsburgh, Pennsylvania 15213-1863, Phone: 412-623-7764, Fax: 412-623-7761, rws9@pitt.edu.
+Current Address: Ludwig Institute for Cancer Research, University of California School of Medicine San Diego, 9500 Gilman Drive, La Jolla, CA 92093-0669, USA
†These authors contributed equally to this work.

Author contribution: EF, EG, JPG, GGP and RWS designed the experiments; EF, EG, ZY, JPG performed the experiments; EF, EG, JPG, GGP, DW, MM, GR and RWS analysed data; PR, JL, TF, MBM and MM contributed new reagents/analytic tools; EF, EG & RWS wrote the paper with comments by ZY, DW, PR, GR, JPG, GGP, MM, BVH.

Disclosure of Potential Conflicts of Interest
RWS is a scientific consultant for Trevigen, Inc. The remaining authors state that there is no conflict of interest.

PAR-interactome after DNA damage and identified hexokinase 1 (HK1) as a PAR binding protein. HK1 activity is suppressed following nuclear ARTD1 activation and binding by PAR. These findings help explain how prolonged activation of ARTD1 triggers energy collapse and cell death, revealing new insight on the importance of nucleus to mitochondria communication via ARTD1 activation.

Keywords

PARP; DNA damage; metabolism; glycolysis; Hexokinase 1; NAD^+; ATP; ARTD1

Introduction

The human genome encodes 17 poly(ADP-ribose) polymerase (PARP) or ADP-ribosyltransferase diphtheria toxin-like (ARTD) proteins that are involved in regulating a variety of cellular processes including DNA damage signalling and repair, chromatin remodeling, transcription, epigenetic gene regulation, mitosis and differentiation (Hassa et al., 2006). All of the catalytically active members of the ARTD/PARP family consume NAD^+ to catalyze ADP-ribosylation of their target substrates but are classified as mono- or poly-(ADP-ribosyl) transferases depending on their ability to transfer monomers or polymers of ADP-ribose (Hottiger et al., 2010). In particular, poly(ADP-ribosyl)ation is known for its switch-like effects on acceptor proteins by virtue of its high charge density and steric hindrance. As a consequence, this post-translational modification can activate or inhibit protein functions, disrupt or promote protein-protein interactions or facilitate protein sub-cellular re-localization (Hottiger et al., 2010).

ADP-ribosyltransferase diphtheria toxin-like 1 (ARTD1 or PARP1) primarily functions as a key enzyme of the base excision repair (BER) and single strand break repair (SSBR) pathways (Almeida and Sobol, 2007). ARTD1 participates in additional DNA repair pathways such as non-homologous end-joining (NHEJ), nucleotide excision repair (NER), in sensing and repairing DNA double-strand breaks and is suggested to participate in the excision step during mismatch repair (De Vos et al., 2012). The participation of ARTD1 in these DNA repair pathways depends on its ability to detect and bind to DNA single-strand breaks with high affinity (Langelier et al., 2012). In BER, a strand break is a normal repair intermediate, which is formed following hydrolysis of the DNA backbone by an apurinic/apyrimidinic endonuclease, APE1 (Almeida and Sobol, 2007; Svilar et al., 2011), triggering ARTD1 activation. Upon activation, ARTD1 synthesizes poly-(ADP-ribose) (PAR) that functions as a mechanism of chromatin decondensation and generates a loading platform for the recruitment of the BER machinery to the lesion site, including proteins such as X-ray repair complementing defective repair in Chinese hamster cells 1 (XRCC1), poly (ADP-ribose) glycohydrolase (PARG) and DNA polymerase ß (Polß) (Schreiber et al., 2006; Svilar et al., 2011). Successful recruitment of the downstream BER proteins facilitates repair of the strand-break, suppressing further ARTD1 activity and PAR synthesis (Masson et al., 1998; Tang et al., 2010).

Conversely, unrepaired DNA breaks, resulting from excessive genotoxin exposure and/or from DNA repair defects, leads to persistent ARTD1 activation and cell death (Gottipati et al., 2010; Juarez-Salinas et al., 1979; Tang et al., 2010). Uncontrolled or excessive activation of ARTD1 is responsible for numerous pathological outcomes including streptozotocin-induced pancreatic beta-cell death and the onset of diabetes (Burns and Gold, 2007; Masutani et al., 1999; Pieper et al., 1999) as well as tissue injury from cerebral and myocardial ischemia (Eliasson et al., 1997; Endres et al., 1997; Pieper et al., 2000). In these and other mouse model studies, ARTD1 activation-induced tissue injury results from the accumulation of DNA repair intermediates (Calvo et al., 2013).

Cell death due to ARTD1 activation was originally suggested to involve energy metabolite (NAD^+ and ATP) depletion (Berger, 1985; Berger et al., 1983; Jacobson et al., 1980). However, the molecular mechanisms underlying ARTD1 hyper-activation-induced ATP depletion and the resulting cell death are unresolved. Confounding this issue, cell type and in particular cellular proliferation status, has yielded widely disparate observations. In astrocytes, cytosolic NAD^+ depletion resulting from ARTD1 activation is suggested to trigger a glycolytic block that can be rescued by NAD^+ or TCA cycle substrates, such as α-ketoglutarate and pyruvate, (Ying et al., 2002; Ying et al., 2003). Neuronal cell death from ARTD1 activation is triggered by un-regulated PAR synthesis, termed parthanatos (Andrabi et al., 2008) and has been suggested to play a role in multiple experimental and physio-pathological scenarios, including stroke, diabetes, inflammation and neurodegeneration. Some reports demonstrate a direct link between ARTD1 hyper-activation and mitochondrial dysfunction, notably through the loss of NAD^+ that precedes the induction of the mitochondrial depolarization and mitochondria outer membrane permeability transition (Alano et al., 2004; Cipriani et al., 2005). In contrast, in apoptosis-deficient cells, it is suggested that only cells relying on glycolysis are sensitive to DNA damage-mediated ARTD1 hyper-activation and necrotic cell death (Zong et al., 2004).

Herein, we tested the hypothesis that the glycolytic block and loss of ATP induced by DNA damage-induced ARTD1 activation is distinct from the resulting loss of NAD^+. In addition, we demonstrate that ARTD1 activation and the resulting synthesis of PAR facilitates the block to glycolysis via regulation/inhibition of PAR binding proteins including the essential glycolytic enzyme hexokinase 1 (HK1).

Results

ARTD1 activation induced by DNA repair intermediates triggers energy metabolite depletion in glioblastoma cells

The acute cellular response to DNA alkylation damage is dependent on the expression of the methyl-specific DNA glycosylase MPG (also known as AAG or ANPG) (Tang et al., 2010) and an imbalance in BER protein expression can lead to an accumulation of toxic DNA repair intermediates (Fu et al., 2012). To evaluate the cellular consequences of DNA damage-induced DNA repair intermediates, we utilised a glioblastoma derived cell line, LN428, with low levels of MPG and the isogenic derivative LN428/MPG over-expressing MPG (see Supplemental text; ***Fig. S1A-D***).

Upon activation, ARTD1 transfers the ADP-ribosyl unit of NAD^+ to synthesize PAR and as a consequence, leads to the rapid loss of total cellular NAD^+. ARTD1 activation also leads to the concomitant loss of ATP and the onset of necrosis (Ha and Snyder, 1999; Tang et al., 2010). Exposure of LN428/MPG cells to MNNG (5μM) results in the loss of close to 90% and 70% respectively, of total cellular NAD^+ and ATP pools with no measureable metabolite depletion observed in the control LN428 cells at this dose of MNNG (***Fig. 1A, 1B***). As expected, pre-treatment with the PARP-inhibitors ABT- 888 or BMN-673 significantly rescues the MNNG-induced NAD^+ loss in the LN428/MPG cells (***Fig. 1C***). Importantly, ARTD1 inhibition completely attenuates the MNNG-induced loss of ATP in LN428/MPG cells (***Fig. 1D, S1K***). To further investigate the involvement of ARTD1 in NAD^+ and ATP loss, we depleted ARTD1 expression using an shRNA coupled with over-expressed MPG via viral transduction of LN428 cells, as described in SI Material and Methods. We verified ARTD1 knockdown and MPG over-expression by RT-PCR and immunoblot (***Fig. S1G, S1H***). PAR synthesis in LN428/ARTD1-KD/MPG cells is largely impaired (***Fig. S1H***) after MNNG even at 10μM, as compared to LN428/MPG cells (***Fig S1D***). Importantly, LN428/ARTD1-KD/MPG cells present no defect in NAD^+ nor ATP levels following MNNG treatment, demonstrating a direct role for ARTD1 in the loss of energy metabolites (***Fig 1C, 1D; grey bars***).

Real-time analysis of ATP levels in gliobastoma cells: ARTD1 activation-mediated ATP depletion initiates in the mitochondria

ATP is generated in both the cytosol and the mitochondria via glycolysis and oxidative phosphorylation, respectively. However, classical measurements of ATP levels lack sub-cellular specificity, limiting the conclusions that can be drawn. To monitor changes in ATP levels in different compartments of living cells as a function of MNNG exposure, LN428 and LN428/MPG cells were transiently transfected with FRET-based ATP sensors, specifically targeted to the mitochondria (AT1.03m), cytosol (AT1.03c) or nucleus (AT1.03n), which produce a YFP FRET signal upon ATP binding (Imamura et al., 2009b). An increase of the CFP/YFP ratio therefore indicates a loss of ATP bound to the FRET sensor. Expression of the FRET-based ATP sensors showed the expected sub-cellular localization measured 48hr post transfection (***Fig. S1I***) and localization was not affected by DNA damaging agent or PARP inhibitor treatment (not shown).

For both the LN428 and LN428/MPG cells, a ten-minute baseline FRET ratio was determined prior to the addition of MNNG (5μM). A low CFP/YFP ratio was observed prior to treatment suggesting normal baseline ATP levels in all subcellular compartments, consistent with whole cell metabolite measurements (***Fig. 1B)***. The different subcellular compartments had slight differences in the absolute starting CFP/YFP ratio and were normalized to 1 at the baseline in order to compare changes between compartments (***Fig. S1J***). Consistent with the whole cell ATP analysis, the CFP/YFP ratio remains close to the baseline in all three sub-cellular compartments for up to 60min after MNNG exposure of the LN428 cells (***Fig. 1E***) indicating that any changes in subcellular ATP due to the minimal PAR formation must be below the sensitivity of the FRET sensors. However, exposure of the LN428/MPG cells to MNNG results in a rapid and dramatic change in the CFP/YFP ratio, in-line with the observed loss of total cellular ATP ***(Fig. 1B, 1F***). Surprisingly, of the

three sub-cellular compartments, an increase in the CFP/YFP ratio (and hence a loss of ATP) was first observed in the mitochondria. The MNNG-induced loss of ATP in the mitochondria began 12min after the start of MNNG treatment, concomitant with the peak of PAR production (***Fig. 1F; S1D***) followed by a decrease in both the cytosolic and nuclear ATP pools, beginning 24min after MNNG exposure (***Fig. 1F; S1I***). In the whole cell ATP analysis, the MNNG-induced loss of ATP in the LN428/MPG cells was completely blocked when ARTD1 was inhibited or depleted (***Fig. 1D***). Similarly, pre-treatment of LN428/MPG cells with the PARP inhibitor was able to rescue the ATP loss in all three sub-cellular compartments (***Fig. S1K, S1L***). These results support an ARTD1-dependent signal that provides a means of intra-cellular communication between the nucleus and the mitochondria in response to genotoxic stress.

Nuclear to mitochondrial communication via ARTD1 activation: DNA damage-induced defects in glycolysis and oxidative phosphorylation

It has been hypothesized that NAD^+ consumption by ARTD1 activation is causative for the rapid depletion of cellular ATP. The kinetics of loss of the mitochondrial, cytosolic and nuclear ATP pools in response to ARTD1 activation suggests that variations in the total cellular level of NAD^+ may signal from the nucleus to the mitochondria by regulating NAD^+-dependent enzymes critical for ATP biosynthesis. To examine this we measured multiple parameters of glycolysis and mitochondrial oxidative phosphorylation in live-cell conditions with the Seahorse XF24 Extracellular Flux Analyzer (SEFA), essentially as described (Qian and Van Houten, 2010; Varum et al., 2011). This real-time, live-cell analysis allows a measure of DNA damage-dependent changes in oxidative phosphorylation (Oxygen Consumption Rate, OCR) and glycolysis (Extracellular Acidification Rate, ECAR). The sequential addition of four metabolic inhibitors: oligomycin, FCCP, 2-deoxyglucose and rotenone allows the calculation of four critical metabolic parameters: (1) the ATP-coupled OCR, (2) the total mitochondrial reserve capacity (TRC), or maximal respiratory rate, (3) the basal ECAR, which corresponds to the basal glycolytic rate and (4) the oligomycin-induced ECAR.

As expected, the isogenic LN428 and LN428/MPG cell lines have similar basal ECAR and OCR profiles (***Fig. 2A, B***; left panels), ideal for comparative analysis. Changes in glycolysis and oxidative phosphorylation were then measured in response to MNNG (1hr, 5μM) and in combination with ARTD1 knockdown or inhibition by pre-treatment with either ABT-888 or BMN-673. In-line with earlier reports using mouse astrocytes (Berger, 1985; Ying et al., 2003), strong ARTD1 activation resulted in the complete loss of glycolysis after MNNG treatment leading to a decrease of both basal and induced ECAR in LN428/MPG but not in LN428 cells (***Fig. 2A; Fig S2A***). Consistent with our hypothesis that the metabolic defects result from ARTD1 activation, ABT-888 or BMN-673 treatment prior to MNNG exposure, leads to a complete rescue of both basal and induced ECAR in LN428/MPG cells (***Fig. 2C; Fig S2A***). Moreover, we show that exposure of LN428/ARTD1-KD/MPG cells to MNNG does not lead to a loss of glycolytic rate as seen in the LN428/MPG cells (***Fig. 2F; Fig. S2D***), providing further evidence for the direct involvement of ARTD1 in this defect of cellular metabolism.

Consistent with the observed loss of NAD^+ and ATP in the LN428/MPG cells in response to MNNG, we found that these cells undergo a complete loss of TRC, with no change to the ATP-coupled OCR (***Fig. 2B***; right panel). The LN428 cells also present with a partial yet significant loss (50%) of TRC in response to MNNG treatment. To determine if the effects observed in both cell lines was the sole result of ARTD1 activation and NAD^+ depletion, the identical analysis was performed with ARTD1 inhibited by pre-treatment with ABT-888 or BMN-673. Interestingly, we observed a complete rescue of TRC in LN428 cells upon ARTD1 inhibition (***Fig. 2E; Fig. S2C***). These data suggest that even a low level of ARTD1 activation (in the case of LN428 cells and illustrated by the anti-PAR immunoblot; ***Fig S1D***) is able to affect the mitochondrial reserve capacity. ARTD1 inhibition is also able to rescue the mitochondrial reserve capacity defect of MNNG-treated LN428/MPG cells (***Fig. 2D, Fig S2B***). To further investigate the role of ARTD1 in MNNG-induced OCR defects, we submitted LN428/ARTD1-KD and LN428/ARTD1-KD/MPG cells to the same treatment and performed the same analysis. As expected, we show that LN428/ARTD1-KD cells do not present the partial defect observed in LN428 cells after MNNG treatment. Expressing MPG in the LN428/ARTD1-KD cells (LN428/ARTD1-KD/MPG) does not trigger a loss of TRC in response to MNNG treatment such as that seen in the LN428/MPG cells (***Fig. 2G***). These results strongly suggest that cellular oxidative phosphorylation, as measured by oxidative reserve capacity, is extremely sensitive to ARTD1 activation. The same results have been observed in HeLa cells treated with increasing doses of MNNG, demonstrating that the MNNG induced metabolic defects are not glioblastoma specific nor an artefact of MPG overexpression, but applicable to multiple cell types (***SI Text and Fig. S2F-J***). From this data, we hypothesize that ARTD1 activation acts as the initiating signal from the nucleus to mediate suppression of both glycolytic and mitochondrial oxidative phosphorylation activity.

NAD^+ depletion is not sufficient to decrease glycolysis or cellular ATP levels

One of the strongest phenotypes associated with ARTD1 activation is an acute loss of NAD^+, with 90% of the cellular NAD^+ content lost within one hour (***Fig. 1A***). Therefore, a likely candidate to signal ARTD1 activation in the nucleus to the metabolic machinery in the mitochondria is the change in overall NAD^+ content. To test this hypothesis, we directly reduced NAD^+ levels in the absence of ARTD1 activation. To inhibit NAD^+ biosynthesis, LN428/MPG cells were treated with FK866, a selective small molecule inhibitor of the essential NAD^+ biosynthesis enzyme nicotinamide phosphoribosyltransferase (NAMPT) (***Fig. 3A***) (Hasmann and Schemainda, 2003). After a 24hr treatment with FK866 (10nM) the NAD^+ pool decreased by about 75%, roughly equivalent to the NAD^+ loss after ARTD1 activation (***Fig. 3B***). Surprisingly, however, ATP levels remained constant and viability was not affected in LN428/MPG cells after treatment with FK866 (***Fig. 3C, S3A***).

Consistent with a role for NAD^+ as a cofactor in mitochondrial enzymatic reactions, FK866 treated cells displayed a significant decrease in total mitochondrial reserve capacity (***Fig. 3D; Fig S3B***). Surprisingly, NAD^+ depletion by FK866 treatment had no effect on either the basal or induced ECAR, unlike MNNG treatment (***Fig. 3E; Fig. S3C***). To demonstrate specificity and selectivity of FK866, treated cells were also supplemented with nicotinamide riboside (NR), a precursor that does not require NAMPT for conversion to NAD^+ (***Fig. 3A***).

NR was synthesized and purified as described in the SI Materials and Methods (***Fig. S4***). As expected, NR pre-treatment could overcome the NAD^+ depletion induced by FK866 (***Fig. 3F***); however, NR did not prevent the loss of NAD^+ or ATP after MNNG even at a 10-fold higher dose (***Fig. 3F, 3G***). Consistently, the FK866-induced loss of TRC is completely rescued by NR (***Fig. 3H, S3D***) but NR was unable to rescue the OCR and ECAR defects in LN428/MPG cells treated with MNNG (***Fig. 3H, I; Fig. S3D and S3E***). Yet, at low doses of MNNG, NR pre-treatment was able to partially rescue NAD^+ levels (***Fig. S3F***). Interestingly, this partial rescue was not sufficient to overcome the OCR and ECAR defects (**Fig. S3G, S3H**) suggesting a more complex effect of ARTD1 activation on cellular metabolism. The sensitivity of oxidative phosphorylation but not glycolysis to direct depletion of NAD^+, suggests that ARTD1 mediated consumption of NAD^+, is a major contributor to the DNA damage-induced loss of oxidative phosphorylation, but inhibition of glycolysis occurs through another unknown mechanism of ARTD1 activation

PARG knockdown rescues the glycolytic defect in MNNG treated cells

The nucleo-cytoplasmic translocation of PAR has been extensively described (Andrabi et al., 2006). As an example, it has been demonstrated that the movement of PAR into the cytosol triggers the release of the mitochondrial protein AIF upon binding of PAR to the AIF PAR-binding motif (PBM) (Yu et al., 2006). This phenomenon has recently been shown to require the endo- and exo-glycohydrolase activities of PARG (Mashimo et al., 2013; Wang et al., 2011; Yu et al., 2002). To investigate whether the glycolytic defects observed herein are due to a release of PAR polymers synthesized by ARTD1 hyper-activation, we stably depleted PARG in LN428 cells (***Fig. S5A***). As expected, the absence of PARG elevates the steady-state level of PAR in response to MNNG treatment (***Fig. S5B***). The global NAD^+ pool was depleted to a greater degree in LN428/PARG-KD cells than in LN428 cells when exposed to increasing concentrations of MNNG but the global ATP pool was not reduced (***Fig. 4A*** **and** ***4B***). As predicted by the loss of NAD^+ following MNNG treatment, we observed a dose dependent decrease of TRC in both the LN428 and LN428/PARG-KD cell lines (***Fig. 4C; S5C***). In-line with a role for PARG in the PAR-mediated ATP loss, the oligomycin-induced ECAR is stable in the LN428/PARG-KD cells but decreases in the LN428 cells (***Fig. 4D; S5D***). Together, these data suggest that loss of PARG (LN428/PARG-KD cells) confers resistance to the glycolytic block induced by ARTD1 activation and implicates PARG (via PAR hydrolysis) in the crosstalk between the nucleus and the mitochondria.

PAR interactome following MNNG-induced accumulation of BER intermediates

Since NAD^+ biosynthesis inhibition is not sufficient to decrease glycolysis and the block to glycolysis is impacted by PARG expression, we hypothesized that ARTD1 activation and the subsequent production of PAR might be causing the inhibition of glycolysis. We therefore sought to examine proteins that interact with or are modified by PAR following induction by MNNG treatment. We reasoned that the “PAR interactome“ would provide insight into the relationship between ARTD1 activation and the loss of glycolysis. We used a specially designed cell line in which Polß is disrupted by shRNA-mediated knockdown and re-expressed with its catalytically dead form (5’deoxyribose phosphate, 5’dRP, lyase Polß mutant K72A). We reasoned that enhanced and persistent BER intermediates and

higher activation of ARTD1 in the isogenic cell line LN428/MPG/Polß-KD/Flag-Polß(K72) at MNNG doses 20-fold lower than that used in earlier proteome-wide analyses would provide an ideal platform to identify PAR-modified and PAR-interacting proteins resulting from MNNG exposure.

Exposure of LN428/MPG/Polß-KD/Flag-Polß(K72) cells to MNNG (5μM, 5min) and isolation of PAR-containing complexes through antibody-based affinity purification was done essentially as described (Gagne et al., 2008; Gagne et al., 2012) (***Fig. S6A***). Proteins either covalently modified by PAR or those in a multi-protein complex with PAR were identified by liquid-chromatography tandem mass spectrometry (LC-MS/MS) to establish a PAR-interactome in response to MNNG (Fig. S6B and Supplementary MS Excel and Scaffold database files). As would be expected, the majority of the proteins identified are DNA repair and DNA damage response proteins, but we also found many novel pathways that are significantly over-represented, including mitochondrial transport and organization, RNA biosynthesis and transcription as well as chromatin assembly (***Fig. S6B and S6C***). Consistent with our findings that ARTD1-activation may have a direct role in altering energy metabolism we also found a significant number of proteins that reside in the mitochondria and function to synthesize metabolic precursors and energy metabolites (***Fig. S6B and S6C***). These include four proteins involved in glycolysis and ATP metabolism: hexokinase 1 (HK1), the mitochondrial channel proteins voltage-dependent anion channels 1 and 2 (VDAC1 & 2) and the ATP/ADP translocase 2, ANT2 (see ***Supplementary MS Excel and Scaffold database files***). For validation, an identical antibody-based affinity-purification workflow was followed by immunoblots for selected proteins to independently confirm the covalently PARylated and PAR-bound protein complexes. Treatment of LN428/MPG/Polß-KD/Flag-Polß(K72) cells yielded the expected PAR-bound complexes including ARTD1, XRCC1, DNA-PKcs and H2B (***Fig. 5A***), as well as DNA ligase III and VDAC1 (***Fig. S6E***). Consistent with the LC-MS/MS analysis, we find that some of the validated proteins are ether bound to or modified by PAR even in the absence of MNNG treatment.

Loss of hexokinase 1 sub-cellular localization and activity due to DNA damage-induced ARTD1 activation

The identification of the HK1/VDAC ATP biosynthesis network in our PAR interactome (***Fig. S6F***) presents the first mechanistic link between ARTD1 activation and DNA damage-induced block to glycolysis, providing a direct confirmation of previous bioinformatics analyses, which suggested that HK1 harbours a PAR-binding motif (PBM) (Gagne et al., 2008). As a validation of our proteomic screen, we found that an elevated level of HK1 was in a complex with PAR upon MNNG treatment (***Fig. 5B***). Reverse IP analysis was used to confirm whether HK1 is modified directly by PAR or is a PAR binding protein. EGFP-tagged HK1 as well as EGFP-tagged XRCC1 or EGFP as a positive and negative control, respectively were expressed in LN428/MPG cells (***Fig. 5C***). While IP of EGFP-tagged XRCC1 shows PAR covalent modification (***Fig. 5C***, *last lane*), neither EGFP nor EGFP-tagged HK1 show PAR modification after immunoblot (***Fig. 5C***, first and middle lane), supporting the conclusion that the identity of HK1 in our PAR-interactome is more likely

the result of an HK1/PAR complex forming via a PBM and not a covalent modification of HK1 by PAR.

The alignment of HK1 with *bona fide* PAR binding motifs from histones H2A, H2B, H3, H4B (known to encode very strong PBMs), XRCC1 (Pleschke et al., 2000), the mitochondrial protein AIF (Wang et al., 2011; Yu et al., 2006; Yu et al., 2002), the stress signalling protein DEK (Fahrer et al., 2010; Kappes et al., 2008), the experimentally validated PBM within hnRNP-A1 (Gagne et al., 2003; Ji et al., 2013; Ji and Tulin, 2009), and Werner syndrome protein (Popp et al., 2013), supports that HK1 encodes a PBM (***Fig. 6A***). To confirm, we spotted purified BSA, histone H2B and HK1 (0.5, 1 and 2μg) on a nitrocellulose membrane and incubated in renaturating buffer containing *in vitro* synthesized PAR and analysed by a PAR immunoblot (***Fig. 6B***). As a control experiment, the spotted proteins were incubated in renaturating buffer without PAR (***Fig. S6G***). As expected, BSA does not bind PAR whereas histone H2B presents a strong PAR-binding signal. More importantly, we find that HK1 also binds PAR. However, mutation of three essential amino residues within the HK1-PBM to alanine (***Fig. 6A***) reduces PAR binding to background levels (***Fig. 6C***). Further, a far-westernblot with these IP extracts shows no additional PAR binding proteins, indicating the PAR-binding signal in the slot-blot derives from an interaction between PAR and HK1 (***Fig. S6H***). We suggest from these studies that the interaction between HK1 and PAR is not a covalent interaction and that HK1 encodes a PBM that when mutated no longer binds PAR.

We hypothesized that ARTD1 activation and the release of PAR by PARG may alter ATP biosynthesis through PAR binding to HK1. HK1 catalyses the first step of glycolysis by phosphorylating glucose and generating glucose-6-phosphate. HK1 interacts with the outer mitochondrial membrane protein VDAC and the disruption of its interaction leads to a decrease in the rate of glycolysis (Shoshan-Barmatz and Golan, 2012), presumably due to either an allosteric effect or a decrease in the availability of VDAC transported ATP. To visualize HK1 sub-cellular localization, we expressed HK1 in the LN428/MPG cells as a fusion with EGFP. Under normal conditions HK1 is localized on the mitochondria and co-localised with the mitochondrial protein Tom20. (***Fig. 6DS6I***). However, after MNNG treatment, localization of HK1 is also cytoplasmic (***Fig. 6D***). In a parallel evaluation, we characterized the localization of HK1 by a biochemical analysis. In untreated cells, very little HK1 is localized to the cytosol, (***Fig. 6E***). However, MNNG treatment induces a significant increase in cytosolic HK1 re-localization (***Fig. 6E, upper panel***) with little to no observed cytosolic HK1 re-localization in LN428 cells (***Fig. 6E, lower panel, Fig. S1D***). Further, we observed that the MNNG-induced cytosolic HK1 re-localization is suppressed by pre-treatment with the ARTD1 inhibitor ABT-888 or by mutation of the HK1 PAR-binding motif, HK1/PBM (***Fig. S6J***). Moreover, HK1 activity was found to be 3-fold lower in LN428/MPG cells treated with MNNG than in untreated cells and HK1 activity was restored by ARTD1 inhibition or knockdown (***Fig. 6F***), indicating a role of ARTD1 hyper-activation in HK1 inactivation. It is noteworthy that even a 3-fold higher dose of MNNG does not lead to HK1 activity alteration in LN428/ARTD1KD/MPG cells (***Fig. 6F***). Interestingly, MNNG treatment of LN428 cells leads to a slight HK1 activity decrease yet not to the same extent as in LN428/MPG cells (***Fig. 6G, upper panel***) and the knockdown of

PARG partially rescues these defects (**Fig 6G lower panel)**. Further, we measured HK1 activity after incubation of purified HK1 with 50 or 100pmol of *in vitro* synthesized PAR (***Fig. 6H***) and observed a progressive decrease in HK1 activity with increasing doses of PAR, demonstrating a direct role of ARTD1 in HK1 inactivation.

Together, these results support our hypothesis that HK1 is a direct target of ARTD1-activation. Once activated, ARTD1-induced PAR is released from the nucleus via PARG activity. In turn, the DNA damage induced loss of ATP biosynthesis can be mediated by release of HK1 from the mitochondrial membrane into the cytosol and PAR-mediated inhibition of HK1 activity. In total, the result is a block to glycolysis.

DISCUSSION

While cell death induced by ARTD1 hyper-activation is well documented, the precise mechanism underlying this observed phenotype remains unresolved and is still a matter of debate. In this study, we demonstrate that ARTD1 induced NAD^+ depletion is not the only factor to mediate metabolic collapse and induce cell death. On the contrary, we show an unambiguous, direct role of ARTD1, through the induction of PAR and the inhibition of hexokinase 1 activity, clarifying the mechanism of ARTD1-directed metabolic collapse. Most importantly, our study brings new insight on the importance of the crosstalk between nuclear ARTD1 activity and other cell compartments, particularly the mitochondria (Andrabi et al., 2008).

It is well established that PAR produced after DNA damage is a key intermediate that triggers a cascade of events leading to cell death. One of these events, initially postulated “PARP assisted cell suicide“, attempts to explain the observed cell death by speculating that NAD^+ depletion caused by ARTD1 hyperactivity causes a shut-down of NAD^+/NADH dependent metabolic pathways followed by ATP depletion and the onset of necrosis (Berger et al., 1983; Ha and Snyder, 1999; Vyas et al., 2013). In line with this theory, we report a significant energy defect in DNA damaged cells due to ARTD1 hyper-activation. We have used two state-of-the-art techniques in live cells to show that incomplete repair of MNNG-induced DNA damage causes a massive increase in ARTD1 activity and a subsequent decline in ATP supplied from both oxidative phosphorylation and glycolysis. While others have reported a decrease of the mitochondrial membrane potential (Juarez-Salinas et al., 1979; Leung et al., 2012), we have been able to measure a loss of total mitochondrial reserve capacity (TRC), a mitochondrial defect, which evaded detection in past studies using mitochondrial extracts

Glycolysis and the tricarboxylic acid (TCA) cycle are the two main NAD^+ consuming pathways in cells, as well as the major NADH providers to the respiratory chain to produce ATP. While the shutdown of these pathways by ARTD1 hyper-activation-mediated NAD^+ loss could explain the respiratory defects in cells exposed to DNA damage, loss of NAD^+ production by direct enzymatic inhibition of NAMPT using FK866 did not cause a decrease in glycolysis. Since these data are in contrast to current models (Alano et al., 2010), we demonstrate for the first time that the glycolytic block upon MNNG treatment is not a mere consequence of NAD^+ loss. Rather, we speculate that ARTD1 hyper-activation has a direct

effect on glycolysis via PAR. This hypothesis is further supported by the lack of a glycolysis rate rescue after NAD^+ synthesis precursor pre-treatment, whereas ARTD1 inhibition by ABT-888 or BMN-673 as well as ARTD1 knockdown, restores glycolysis.

Consistent with our hypothesis that ARTD1 directly affects glycolysis, we identified the glycolytic protein Hexokinase 1 (HK1), the enzyme responsible for the first step of glycolysis, as a potential PAR binding protein by mass spectrometry. We find that while HK1 is not covalently modified by ARTD1, HK1 binds PAR through a PBM earlier identified by mass spectrometry analysis (Gagne et al., 2008). HK1 is one of the three major isoenzymes of the hexokinase family. HK1 is mainly associated with the outer mitochondrial membrane through an interaction with the channel protein VDAC, also identified in our PAR binding protein mass spectrometry analysis (see ***Supplementary MS Excel and Scaffold database files***) (Jun et al., 2012; Wilson, 2003). This physical interaction couples cytosolic glycolysis to mitochondrial oxidative phosphorylation by which the cells produce most of their ATP and potentially links ARTD1 activity and PAR to the metabolic events in the mitochondria. Indeed, a previous study has demonstrated that during ischemic renal injury, ARTD1 can poly(ADP-ribosyl)ate and inhibit glyceraldehyde-3-phosphate-dehydrogenase (GAPDH), the enzyme responsible for the catalysis of the second step of glycolysis (Devalaraja-Narashimha and Padanilam, 2009). We also observed that GAPDH is bound or modified by PAR but at an extremely low level, suggesting that the PAR-interactome we have identified may be selective for a cellular response to BER intermediates (see ***Supplementary MS Excel and Scaffold database files***). Our PAR binding protein mass spectrometry analysis also identified 3 enzymes involved in the Krebs cycle (succinate dehydrogenase, alpha-ketoglutarate dehydrogenase and pyruvate dehydrogenase) suggesting a possible role of ARTD1 in the regulation of these enzyme activities after DNA damage. Consistent with this idea, we found that although NR pre-treatment is able to partly rescue the global NAD^+ pool after MNNG treatment at low doses, both the TRC and ECAR were still affected (***Fig S4G, H***). Ying et al. previously demonstrated that treatment of murine astrocytes after MNNG with tricarboxylic acid (TCA) cycle intermediates partly rescued cell death (Ying et al., 2002). These results confirm our observation that ARTD1 hyper-activation is directly involved in the inhibition of glycolysis after MNNG treatment and does not exclude the possible involvement of ARTD1 in the control of the TCA cycle enzymes.

MNNG induced ARTD1 hyper-activation could negatively affect glycolysis by creating excess PAR able to migrate into the cytosol and bind to HK1 and thus, inhibit its enzyme activity. In support of this hypothesis, we find that the ECAR values of LN428/PARG-KD cells are more resistant to MNNG than LN428 cells. In addition, we observe a decrease in HK1 activity in LN428/MPG cell lysates after MNNG treatment that is rescued by ARTD1 inhibition, and more importantly a direct effect of HK1 activity upon *in vitro* incubation with PAR. These two key results constitute strong evidence for a role of ARTD1 in controlling HK1 activity under cellular stress. Interestingly, some studies correlate HK1 sub-cellular localisation and activity. It has been demonstrated that the release of HK1 can affect its activity (Saraiva et al., 2010). HK1 release from the mitochondria may also be responsible for a decrease in the mitochondrial membrane potential and can promote TNF-

induced apoptosis in HeLa cells (Ullu et al., 2002). Intriguingly, we find a mobilization of HK1 from the mitochondria to the cytosol after MNNG treatment in LN428/MPG cells, consistent with the observed reduction of HK1 activity.

These findings suggest a working model in which ARTD1 hyper-activation leads to inhibition of HK1 and mis-localization of HK1 from the outer mitochondrial membrane, leading to a reduction in cellular glycolysis and a depletion in cellular ATP pools. This effect of ARTD1 activity coupled with NAD^+ depletion might explain the cell sensitivity in response to DNA alkylation damage and the resulting ARTD1 activation that is induced due to un-repaired DNA strand breaks and BER intermediates. PAR could affect HK1 activity in two non-mutually exclusive ways. Firstly, PAR binding to HK1 could cause a decrease in its affinity to VDAC causing its migration into the cytoplasm. Secondly, PAR binding could allosterically affect HK1 activity. Data presented here support both mechanisms. Furthermore, high-resolution crystal structures indicate that the putative PBM of HK1 is located in an accessible surface area that overlaps with a helix in its N-terminal domain (Rosano, 2011). This helical domain is involved both in the binding of ATP and in the interaction of HK1 with the mitochondrial protein channel VDAC1, making both scenarios plausible.

After submission of this manuscript, another group reported that mouse cortical neurons treated with high dose MNNG undergo ARTD1-dependent energy depletion that is mediated by glycolysis inhibition (Andrabi et al., 2014). The authors hypothesize that PAR induced release of AIF could be responsible for the ARTD1-activation induced decrease in HK1 activity via the loss of an interaction between both proteins. Further to this point, we demonstrate the ARTD1 activation-dependent release of HK1 into the cytosol, previously suggested as being responsible for HK1 inhibition (Saraiva et al., 2010). In addition to demonstrating the PAR-dependent release of HK1, we also show that the HK1-PBM is required for ARTD1-activation induced inhibition of HK1, implicating binding of PAR to HK1 as a requisite event. Future studies will reveal the role of PAR in the regulation of HK1 and the contribution of this interaction to the loss of glycolysis, mitochondrial dysfunction and the onset of parthanatos in response to genotoxin exposure.

In summary, we propose a model in which DNA repair intermediates induce ARTD1 hyper-activation. In turn, the resulting PAR synthesis leads to a release of PAR units in the cytoplasm, which upon binding to HK1 causes the decrease of its activity and/or its dissociation from VDAC, leading to its release into the cytoplasm and a subsequent decrease in its activity. Such a model, in which PAR would be required to migrate from the nucleus to the mitochondria, is consistent with a role for both PARG and the ADP-ribosylhydrolase like 2 protein (ARH3) regulating such a response, as recently suggested (Mashimo et al., 2013). Data presented in this study therefore provide a novel molecular mechanism linking DNA damage induced ARTD1 hyperactivation to cell death through the direct inhibition of glycolysis by diminishing HK1 activity. These data are in contrast to the previously proposed ‘secondary shutdown’ of the glycolytic pathway by ARTD1-mediated NAD^+ depletion. Our findings have wide ranging implications not only for the fields of DNA repair, BER and chemotherapy, but also for diseases where ARTD1 activation plays a

prominent role, such as ischemic injury after stroke or myocardial infarction, traumatic brain injury, Parkinson's disease and septic shock.

Experimental Procedures

More details on the Experimental Procedures are provided in the Supplemental Experimental Procedures section.

Cell culture

The cell line LN428 has been established as previously reported and LN428/MPG cells were prepared and cultured as described (Tang et al., 2010). LN428/ARTD1-KD/copGFP, LN428/ARTD1-KD/MPG-copGFP, LN428/MPG/PARG-KD and LN428/PARG-KD cells are stable cell lines developed by lentiviral transduction, essentially as described (Goellner et al., 2011; Svilar et al., 2012; Tang et al., 2010).

Cell cytotoxicity

MNNG- and FK866-induced cytotoxicity was determined by an MTS assay, a modified MTT assay as described previously (Tang et al., 2010).

Hexokinase activity

Hexokinase activity of purified protein and from cell lysates was measured using the Hexokinase Colorimetric Assay (BioVision Inc.).

Global NAD^+ and ATP measurements

Global NAD^+ and ATP pools were measured using the EnzyChrom NAD^+/NADH Assay kit (BioAssay Systems) and the ATP lite assay kit (Perkin-Elmer), respectively.

Subcellular ATP analysis

Subcellular ATP levels were evaluated by fluorescence resonance energy transfer (FRET) using the ATeam probes composed of mVenus and mseCFP linked to the ε subunit of Bacillus subtilis F_0F_1-ATP synthase (Imamura et al., 2009a) and targeted to the three different cell compartments.

Metabolic flux measurement

The oxygen consumption rates (OCR) and extracellular acidification rates (ECAR) were measured using the Seahorse Extracellular Flux Analyzer (Seahorse Bioscience), essentially as described (Furda et al., 2012; Qian and Van Houten, 2010; Varum et al., 2011).

PAR dot blot and far western blot

PAR was synthesized *in vitro* as previously described (Ame et al., 2009) or obtained in purified form from Trevigen (#4336-100-01). Purified proteins (BSA, H2B or HK1; 0.5, 1 or 2μg) were spotted on a nitrocellulose membrane and incubated in renaturing buffer containing PAR polymers. Presence of bound PAR was then detected by immunoblot using the 10H anti-PAR antibody. For the far western blot, GFP-tagged proteins were expressed in

LN428 cells, isolated using GFP-Trap (Chromotek) beads and resolved by SDS-PAGE followed by transfer to a nitrocellulose membrane. The membrane was incubated in renaturing buffer as described above and the PAR signal was detected using 10H antibody conjugated to biotin, followed by incubation with streptavidin-HRP.

Immunoprecipitation

LN428/MPG/Polß-KD/FLAG-Polß(K72A) or LN428/MPG cells were seeded onto 15mm dishes and grown to 80-90% confluence. Cells were either treated with ABT-888 (10μM, 1hr) and/or with MNNG (5μM, 5min) and then cell lysates were prepared for immunoprecipitation with either the 10H anti-PAR Ab or the GFP-Trap (Chromotek).

Immunofluorescence and confocal microscopy

Cells were seeded on glass coverslips for 24hr before MNNG treatment during the time indicated preceded by PJ34 (or vehicle) pre-treatment. The immunodetection of PAR was performed as previously described (Ame et al., 2009). For immunodetection of HK1-GFP, cells were modified to express HK1-GFP by transfection with pEGFP-N3-FLHK1 (AddGene) using the transfection reagent JetPrime (VWR) 24hr prior to the cell treatment and fixation for immunofluoresence. To visualize the mitochondria, an antibody against the membrane protein Tom20 has been used (SantaCruz).

Mass spectrometry

After immunoprecipitation of the PAR binding complexes, Mass Spectrometry analyses were performed on a TripleTOF® 5600 mass spectrometer fitted with a nanospray III ion source (ABSciex, Concord, ON) and coupled to an Agilent 1200 HPLC (extensive details are reported in SI).

Supplementary Material

Refer to Web version on PubMed Central for supplementary material.

Acknowledgement

This work was supported by grants from the National Institute of Health (NIH) [CA148629, GM087798, ES019498, ES021116, GM099213 and CA148629-04S1] to RWS, from the Canadian Institutes of Health Research (CIHR) [MOP-178013; MOP-209278] to GGP and from PA CURE to BVH. Support for the synthetic chemistry conducted by PR was provided by the John King Laboratory Funds. Support was also provided by the University of Pittsburgh Department of Pharmacology & Chemical Biology through a Pharmacology Fellowship to EMG. GGP holds a Tier1 Canada Chair in Proteomics. BVH holds the Richard M. Cyert Chair as Professor of Molecular Oncology. Support for the UPCI Lentiviral (Vector Core) Facility and the UPCI Cell and Tissue Imaging Facility was provided in part by the Cancer Center Support Grant from the National Institutes of Health [P30CA047904].

References

Alano CC, Garnier P, Ying W, Higashi Y, Kauppinen TM, Swanson RA. NAD+ depletion is necessary and sufficient for poly(ADP-ribose) polymerase-1-mediated neuronal death. J Neurosci. 2010; 30:2967–2978. [PubMed: 20181594]

Alano CC, Ying W, Swanson RA. Poly(ADP-ribose) polymerase-1-mediated cell death in astrocytes requires NAD+ depletion and mitochondrial permeability transition. J Biol Chem. 2004; 279:18895–18902. [PubMed: 14960594]

Almeida KH, Sobol RW. A unified view of base excision repair: lesion-dependent protein complexes regulated by post-translational modification. DNA Repair. 2007; 6:695–711. [PubMed: 17337257]

Ame JC, Hakme A, Quenet D, Fouquerel E, Dantzer F, Schreiber V. Detection of the nuclear poly(ADP-ribose)-metabolizing enzymes and activities in response to DNA damage. Methods Mol Biol. 2009; 464:267–283. [PubMed: 18951190]

Andrabi SA, Dawson TM, Dawson VL. Mitochondrial and nuclear cross talk in cell death: parthanatos. Ann N Y Acad Sci. 2008; 1147:233–241. [PubMed: 19076445]

Andrabi SA, Kim NS, Yu SW, Wang H, Koh DW, Sasaki M, Klaus JA, Otsuka T, Zhang Z, Koehler RC, et al. Poly(ADP-ribose) (PAR) polymer is a death signal. Proc Natl Acad Sci U S A. 2006; 103:18308–18313. [PubMed: 17116882]

Andrabi SA, Umanah GK, Chang C, Stevens DA, Karuppagounder SS, Gagne JP, Poirier GG, Dawson VL, Dawson TM. Poly(ADP-ribose) polymerase-dependent energy depletion occurs through inhibition of glycolysis. Proc Natl Acad Sci U S A. 2014; 111:10209–10214. [PubMed: 24987120]

Berger NA. Poly(ADP-ribose) in the cellular response to DNA damage. Radiat Res. 1985; 101:4–15. [PubMed: 3155867]

Berger NA, Sims JL, Catino DM, Berger SJ. Poly(ADP-ribose) polymerase mediates the suicide response to massive DNA damage: studies in normal and DNA-repair defective cells. Princess Takamatsu Symp. 1983; 13:219–226. [PubMed: 6317637]

Burns N, Gold B. The effect of 3-methyladenine DNA glycosylase-mediated DNA repair on the induction of toxicity and diabetes by the beta-cell toxicant streptozotocin. Toxicol Sci. 2007; 95:391–400. [PubMed: 17098815]

Calvo JA, Moroski-Erkul CA, Lake A, Eichinger LW, Shah D, Jhun I, Limsirichai P, Bronson RT, Christiani DC, Meira LB, et al. Aag DNA glycosylase promotes alkylation-induced tissue damage mediated by Parp1. PLoS Genet. 2013; 9:e1003413. [PubMed: 23593019]

Cipriani G, Rapizzi E, Vannacci A, Rizzuto R, Moroni F, Chiarugi A. Nuclear poly(ADP-ribose) polymerase-1 rapidly triggers mitochondrial dysfunction. J Biol Chem. 2005; 280:17227–17234. [PubMed: 15750180]

De Vos M, Schreiber V, Dantzer F. The diverse roles and clinical relevance of PARPs in DNA damage repair: current state of the art. Biochemical pharmacology. 2012; 84:137–146. [PubMed: 22469522]

Devalaraja-Narashimha K, Padanilam BJ. PARP-1 inhibits glycolysis in ischemic kidneys. J Am Soc Nephrol. 2009; 20:95–103. [PubMed: 19056868]

Eliasson MJ, Sampei K, Mandir AS, Hurn PD, Traystman RJ, Bao J, Pieper A, Wang ZQ, Dawson TM, Snyder SH, et al. Poly(ADP-ribose) polymerase gene disruption renders mice resistant to cerebral ischemia. Nat Med. 1997; 3:1089–1095. [PubMed: 9334719]

Endres M, Wang ZQ, Namura S, Waeber C, Moskowitz MA. Ischemic brain injury is mediated by the activation of poly(ADP-ribose)polymerase. J Cereb Blood Flow Metab. 1997; 17:1143–1151. [PubMed: 9390645]

Fahrer J, Popp O, Malanga M, Beneke S, Markovitz DM, Ferrando-May E, Burkle A, Kappes F. High-affinity interaction of poly(ADP-ribose) and the human DEK oncoprotein depends upon chain length. Biochemistry. 2010; 49:7119–7130. [PubMed: 20669926]

Fu D, Calvo JA, Samson LD. Balancing repair and tolerance of DNA damage caused by alkylating agents. Nat Rev Cancer. 2012; 12:104–120. [PubMed: 22237395]

Furda AM, Marrangoni AM, Lokshin A, Van Houten B. Oxidants and not alkylating agents induce rapid mtDNA loss and mitochondrial dysfunction. DNA Repair (Amst). 2012; 11:684–692. [PubMed: 22766155]

Gagne JP, Hunter JM, Labrecque B, Chabot B, Poirier GG. A proteomic approach to the identification of heterogeneous nuclear ribonucleoproteins as a new family of poly(ADP-ribose)-binding proteins. Biochem J. 2003; 371:331–340. [PubMed: 12517304]

Gagne JP, Isabelle M, Lo KS, Bourassa S, Hendzel MJ, Dawson VL, Dawson TM, Poirier GG. Proteome-wide identification of poly(ADP-ribose) binding proteins and poly(ADP-ribose)-associated protein complexes. Nucleic Acids Res. 2008; 36:6959–6976. [PubMed: 18981049]

Gagne JP, Pic E, Isabelle M, Krietsch J, Ethier C, Paquet E, Kelly I, Boutin M, Moon KM, Foster LJ, et al. Quantitative proteomics profiling of the poly(ADP-ribose)-related response to genotoxic stress. Nucleic Acids Res. 2012; 40:7788–7805. [PubMed: 22669911]

Goellner EM, Grimme B, Brown AR, Lin YC, Wang XH, Sugrue KF, Mitchell L, Trivedi RN, Tang JB, Sobol RW. Overcoming Temozolomide Resistance in Glioblastoma via Dual Inhibition of NAD+ Biosynthesis and Base Excision Repair. Cancer Res. 2011; 71:2308–2317. [PubMed: 21406402]

Gottipati P, Vischioni B, Schultz N, Solomons J, Bryant HE, Djureinovic T, Issaeva N, Sleeth K, Sharma RA, Helleday T. Poly(ADP-ribose) polymerase is hyperactivated in homologous recombination-defective cells. Cancer Res. 2010; 70:5389–5398. [PubMed: 20551068]

Ha HC, Snyder SH. Poly(ADP-ribose) polymerase is a mediator of necrotic cell death by ATP depletion. Proc Natl Acad Sci U S A. 1999; 96:13978–13982. [PubMed: 10570184]

Hasmann M, Schemainda I. FK866, a highly specific noncompetitive inhibitor of nicotinamide phosphoribosyltransferase, represents a novel mechanism for induction of tumor cell apoptosis. Cancer Res. 2003; 63:7436–7442. [PubMed: 14612543]

Hassa PO, Haenni SS, Elser M, Hottiger MO. Nuclear ADP-ribosylation reactions in mammalian cells: where are we today and where are we going? Microbiol Mol Biol Rev. 2006; 70:789–829. [PubMed: 16959969]

Hottiger MO, Hassa PO, Luscher B, Schuler H, Koch-Nolte F. Toward a unified nomenclature for mammalian ADP-ribosyltransferases. Trends Biochem Sci. 2010; 35:208–219. [PubMed: 20106667]

Imamura H, Nhat KP, Togawa H, Saito K, Iino R, Kato-Yamada Y, Nagai T, Noji H. Visualization of ATP levels inside single living cells with fluorescence resonance energy transfer-based genetically encoded indicators. Proc Natl Acad Sci U S A. 2009a; 106:15651–15656. [PubMed: 19720993]

Imamura H, Nhat KP, Togawa H, Saito K, Iino R, Kato-Yamada Y, Nagai T, Noji H. Visualization of ATP levels inside single living cells with fluorescence resonance energy transfer-based genetically encoded indicators. Proceedings of the National Academy of Sciences of the United States of America. 2009b; 106:15651–15656. [PubMed: 19720993]

Jacobson MK, Levi V, Juarez-Salinas H, Barton RA, Jacobson EL. Effect of carcinogenic N-alkyl-N-nitroso compounds on nicotinamide adenine dinucleotide metabolism. Cancer Res. 1980; 40:1797–1802. [PubMed: 6245804]

Ji Y, Jarnik M, Tulin AV. Poly(ADP-ribose) glycohydrolase and poly(ADP-ribose)-interacting protein Hrp38 regulate pattern formation during Drosophila eye development. Gene. 2013; 526:187–194. [PubMed: 23711619]

Ji Y, Tulin AV. Poly(ADP-ribosyl)ation of heterogeneous nuclear ribonucleoproteins modulates splicing. Nucleic Acids Res. 2009; 37:3501–3513. [PubMed: 19346337]

Juarez-Salinas H, Sims JL, Jacobson MK. Poly(ADP-ribose) levels in carcinogen-treated cells. Nature. 1979; 282:740–741. [PubMed: 229416]

Jun BH, Kang H, Lee YS, Jeong DH. Fluorescence-based multiplex protein detection using optically encoded microbeads. Molecules. 2012; 17:2474–2490. [PubMed: 22382526]

Kappes F, Fahrer J, Khodadoust MS, Tabbert A, Strasser C, Mor-Vaknin N, Moreno-Villanueva M, Burkle A, Markovitz DM, Ferrando-May E. DEK is a poly(ADP-ribose) acceptor in apoptosis and mediates resistance to genotoxic stress. Mol Cell Biol. 2008; 28:3245–3257. [PubMed: 18332104]

Langelier MF, Planck JL, Roy S, Pascal JM. Structural basis for DNA damage-dependent poly(ADP-ribosyl)ation by human PARP-1. Science (New York, N.Y. 2012; 336:728–732.

Leung A, Todorova T, Ando Y, Chang P. Poly(ADP-ribose) regulates post-transcriptional gene regulation in the cytoplasm. RNA biology. 2012; 9:542–548. [PubMed: 22531498]

Mashimo M, Kato J, Moss J. ADP-ribosyl-acceptor hydrolase 3 regulates poly (ADP-ribose) degradation and cell death during oxidative stress. Proc Natl Acad Sci U S A. 2013; 110:18964–18969. [PubMed: 24191052]

Masson M, Niedergang C, Schreiber V, Muller S, Menissier-de Murcia J, de Murcia G. XRCC1 is specifically associated with poly(ADP-ribose) polymerase and negatively regulates its activity following DNA damage. Molecular and Cellular Biology. 1998; 18:3563–3571. [PubMed: 9584196]

Masutani M, Suzuki H, Kamada N, Watanabe M, Ueda O, Nozaki T, Jishage K, Watanabe T, Sugimoto T, Nakagama H, et al. Poly(ADP-ribose) polymerase gene disruption conferred mice resistant to streptozotocin-induced diabetes. Proc Natl Acad Sci U S A. 1999; 96:2301–2304. [PubMed: 10051636]

Pieper AA, Brat DJ, Krug DK, Watkins CC, Gupta A, Blackshaw S, Verma A, Wang ZQ, Snyder SH. Poly(ADP-ribose) polymerase-deficient mice are protected from streptozotocin-induced diabetes. Proc Natl Acad Sci U S A. 1999; 96:3059–3064. [PubMed: 10077636]

Pieper AA, Walles T, Wei G, Clements EE, Verma A, Snyder SH, Zweier JL. Myocardial postischemic injury is reduced by polyADPripose polymerase-1 gene disruption. Mol Med. 2000; 6:271–282. [PubMed: 10949908]

Pleschke JM, Kleczkowska HE, Strohm M, Althaus FR. Poly(ADP-ribose) binds to specific domains in DNA damage checkpoint proteins. J Biol Chem. 2000; 275:40974–40980. [PubMed: 11016934]

Popp O, Veith S, Fahrer J, Bohr VA, Burkle A, Mangerich A. Site-specific noncovalent interaction of the biopolymer poly(ADP-ribose) with the Werner syndrome protein regulates protein functions. ACS chemical biology. 2013; 8:179–188. [PubMed: 23082994]

Qian W, Van Houten B. Alterations in bioenergetics due to changes in mitochondrial DNA copy number. Methods. 2010; 51:452–457. [PubMed: 20347038]

Rosano C. Molecular model of hexokinase binding to the outer mitochondrial membrane porin (VDAC1): Implication for the design of new cancer therapies. Mitochondrion. 2011; 11:513–519. [PubMed: 21315184]

Saraiva LM, Seixas da Silva GS, Galina A, da-Silva WS, Klein WL, Ferreira ST, De Felice FG. Amyloid-beta triggers the release of neuronal hexokinase 1 from mitochondria. PLoS ONE. 2010; 5:e15230. [PubMed: 21179577]

Schreiber V, Dantzer F, Ame JC, de Murcia G. Poly(ADP-ribose): novel functions for an old molecule. Nat Rev Mol Cell Biol. 2006; 7:517–528. [PubMed: 16829982]

Shoshan-Barmatz V, Golan M. Mitochondrial VDAC1: function in cell life and death and a target for cancer therapy. Curr Med Chem. 2012; 19:714–735. [PubMed: 22204343]

Svilar D, Dyavaiah M, Brown AR, Tang JB, Li J, McDonald PR, Shun TY, Braganza A, Wang XH, Maniar S, et al. Alkylation sensitivity screens reveal a conserved cross-species functionome. Mol Cancer Res. 2012; 10:1580–1596. [PubMed: 23038810]

Svilar D, Goellner EM, Almeida KH, Sobol RW. Base Excision Repair and lesion-dependent sub-pathways for repair of oxidative DNA damage. Antioxid Redox Signal. 2011; 14:2491–2507. [PubMed: 20649466]

Tang J, Goellner EM, Wang XW, Trivedi RN, St. Croix CM, Jelezcova E, Svilar D, Brown AR, Sobol RW. Bioenergetic Metabolites Regulate Base Excision Repair-Dependent Cell Death in Response to DNA Damage. Molecular Cancer Research. 2010; 8:67–79. [PubMed: 20068071]

Ullu E, Djikeng A, Shi H, Tschudi C. RNA interference: advances and questions. Philosophical transactions of the Royal Society of London. Biological sciences. 2002; 357:65–70. Series B. [PubMed: 11839183]

Varum S, Rodrigues AS, Moura MB, Momcilovic O, Easley C.A.t. Ramalho-Santos J, Van Houten B, Schatten G. Energy metabolism in human pluripotent stem cells and their differentiated counterparts. PLoS ONE. 2011; 6:e20914. [PubMed: 21698063]

Vyas S, Chesarone-Cataldo M, Todorova T, Huang YH, Chang P. A systematic analysis of the PARP protein family identifies new functions critical for cell physiology. Nature communications. 2013; 4:2240.

Wang Y, Kim NS, Haince JF, Kang HC, David KK, Andrabi SA, Poirier GG, Dawson VL, Dawson TM. Poly(ADP-ribose) (PAR) binding to apoptosis-inducing factor is critical for PAR polymerase-1-dependent cell death (parthanatos). Sci Signal. 2011; 4:ra20. [PubMed: 21467298]

Wilson JE. Isozymes of mammalian hexokinase: structure, subcellular localization and metabolic function. The Journal of experimental biology. 2003; 206:2049–2057. [PubMed: 12756287]

Ying W, Chen Y, Alano CC, Swanson RA. Tricarboxylic acid cycle substrates prevent PARP-mediated death of neurons and astrocytes. J Cereb Blood Flow Metab. 2002; 22:774–779. [PubMed: 12142562]

Ying W, Garnier P, Swanson RA. NAD+ repletion prevents PARP-1-induced glycolytic blockade and cell death in cultured mouse astrocytes. Biochem Biophys Res Commun. 2003; 308:809–813. [PubMed: 12927790]

Yu SW, Andrabi SA, Wang H, Kim NS, Poirier GG, Dawson TM, Dawson VL. Apoptosis-inducing factor mediates poly(ADP-ribose) (PAR) polymer-induced cell death. Proc Natl Acad Sci U S A. 2006; 103:18314–18319. [PubMed: 17116881]

Yu SW, Wang H, Poitras MF, Coombs C, Bowers WJ, Federoff HJ, Poirier GG, Dawson TM, Dawson VL. Mediation of poly(ADP-ribose) polymerase-1-dependent cell death by apoptosis-inducing factor. Science. 2002; 297:259–263. [PubMed: 12114629]

Zong WX, Ditsworth D, Bauer DE, Wang ZQ, Thompson CB. Alkylating DNA damage stimulates a regulated form of necrotic cell death. Genes & development. 2004; 18:1272–1282. [PubMed: 15145826]

Highlights

- ARTD1 activation-mediated ATP depletion initiates in the mitochondria
- ARTD1 activation suppresses glycolysis and oxidative phosphorylation
- NAD^+ depletion does not impact glycolysis or cellular ATP levels
- HK1 activity is inhibited by ARTD1 activation to suppress glycolysis

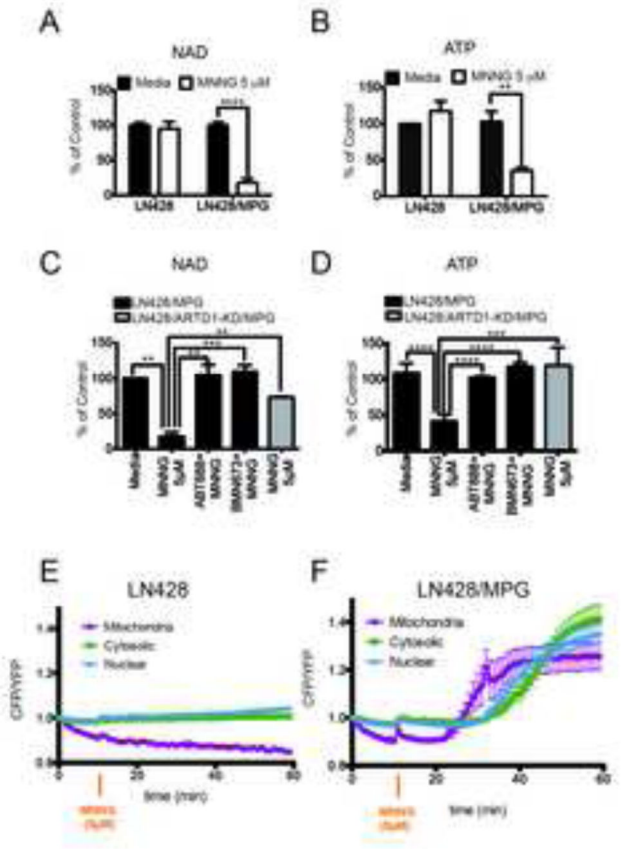

Figure 1. ARTD1 hyper-activation induced by DNA repair intermediates triggers energetic depletion in glioblastoma cells

(A and B) Global NAD^+ (A) and global ATP (B) levels in LN428 and LN428/MPG cells after 1hr treatment with either media or 5μM MNNG. The data shown is the average of 3 independent experiments +/− SD and are reported as percentage of the untreated control cell line (LN428): (A)****p<0.0001 (B) **p=0.01. (C and D) Global NAD^+ (C) and global ATP (D) levels in LN428/MPG cells (black bars) or in LN428/ARTD1-KD/MPG cells (grey bar) after a 1hr treatment with either media, 5μM MNNG or 5μM MNNG after a pre-treatment with ARTD1 inhibitors ABT-888 or BMN673, as indicated. The data shown is the average of 3 independent experiments +/− SD and are reported as percentage of the untreated cells: (C)**p<0.005, ***p=0,0003, (D) ****p<0,0001, ***p<0,001. (E and F) FRET ratio calculated in the compartments of LN428 cells (E) or LN428/MPG cells (F) transfected with the indicated FRET sensors. Images were acquired each minute. A ten-minute baseline period was recorded before cells were treated with 5μM MNNG (orange arrow). FRET traces shown are the mean of 5-7 cells (LN428) or 7-9 (LN428/MPG) +/− SE.

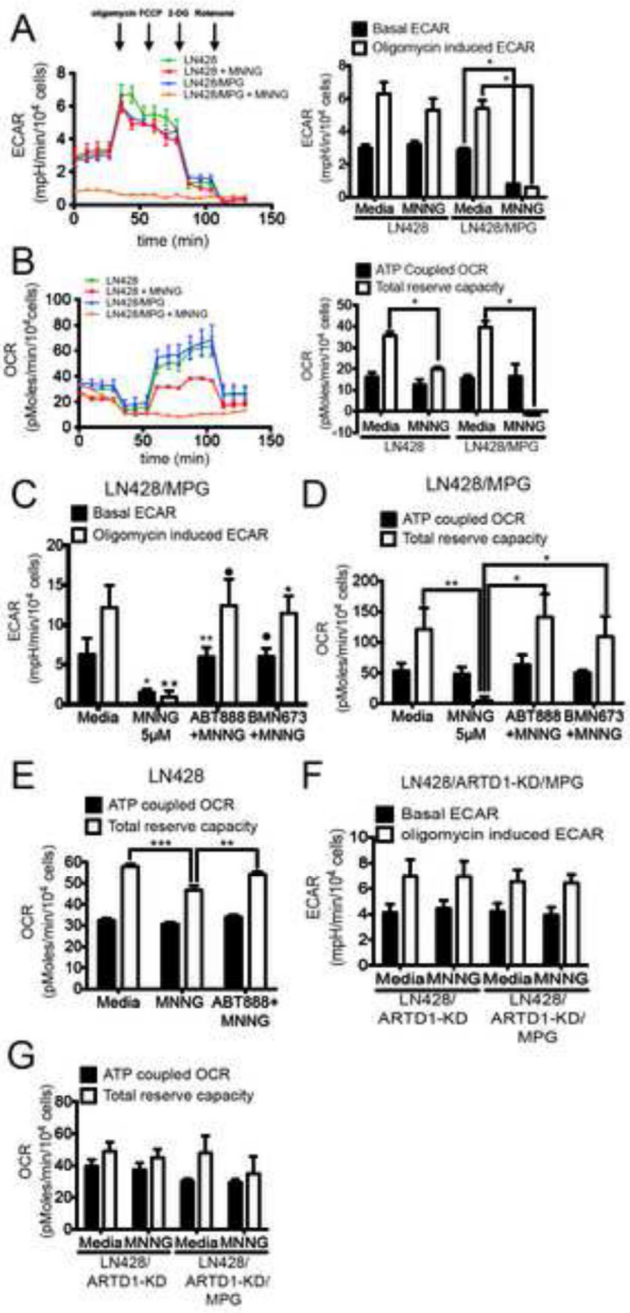

Figure 2. Mitochondrial dysfunction following alkylating agent-induced ARTD1 activation

(A and B) Seahorse extracellular flux analyser (SEFA) measurement of ECAR metabolic profile (A) or OCR metabolic profile (B) in LN428 or LN428/MPG cells treated with either media or MNNG (5μM, 1hr). Bar graphs representing basal ECAR and oligomycin induced ECAR (A) or ATP coupled OCR and total reserve capacity (TRC) (B) are shown on the right. Traces shown are the mean of two independent experiments in which each data point represents technical replicates of 5 wells each +/− SE. Basal and induced ECAR rates, ATP coupled OCR and TRC are calculated using the average of 3 data points collected for each metabolic inhibitor, +/− SD (*p<0.05). (C and D) ECAR measurements (C) and OCR

measurements (D) in LN428/MPG cells treated with 5μM MNNG following pre-treatment with media control or ARTD1 inhibitors ABT-888 or BMN-673 as indicated. Shown is the mean of 3 independent experiments +/− SD as described above: (C)*p<0.05 compared to media for basal ECAR, •p<0,05 compared to MNNG for basal ECAR, **p<0.005 compared to MNNG for basal ECAR, ∗∗p<0.005 compared to media for induced ECAR, •p<0,005 compared to MNNG for induced ECAR, ∗p<0,01 compared to MNNG for induced ECAR; D*p<0.05, **p<0.01. (E) OCR measurement in LN428 cells treated with 5μM MNNG following pre-treatment with media control or ARTD1 inhibitor ABT-888. Shown is the mean of 3 independent experiments +/− SD (***p<0.0004 compared to media control for TRC, **p<0.002 compared to MNNG for TRC). (F and G) ECAR measurement (F) and OCR measurement (G) for LN428/ARTD1-KD or LN428/ARTD1-KD/MPG cells after treatment with media control or 5μM MNNG. Shown is the average of 3 independent experiments +/− SD as described above.

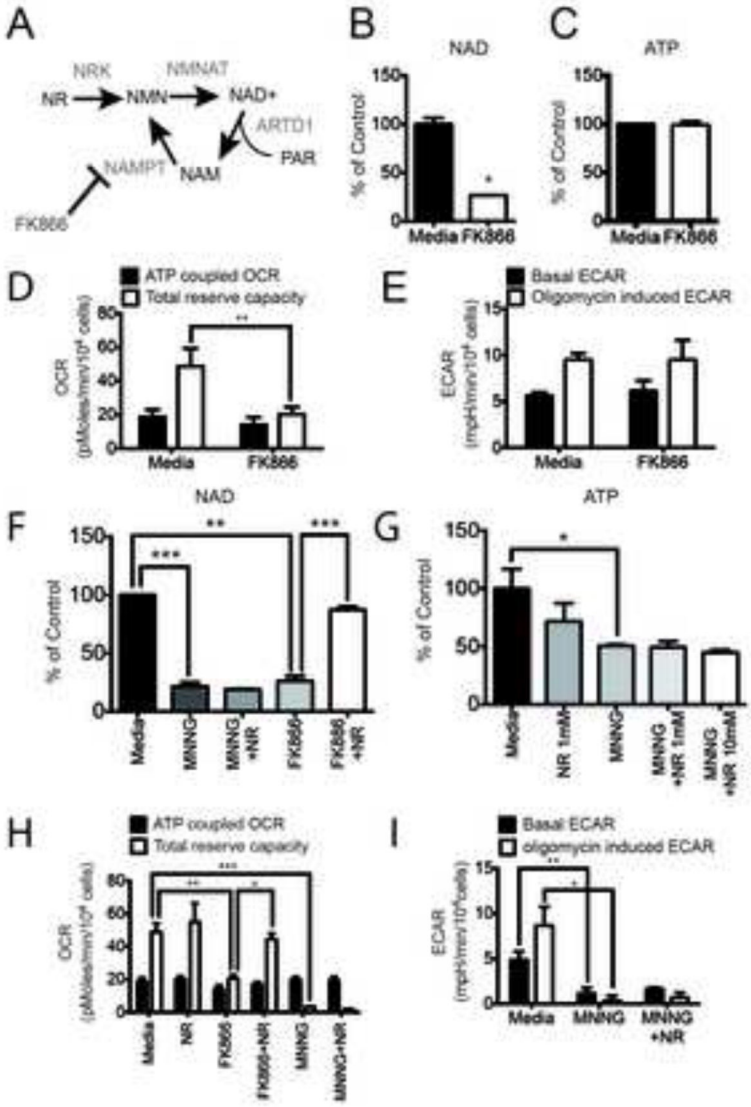

Figure 3. NAD$^+$ depletion does not alter glycolysis in LN428/MPG cells

(A) Schematic of NAD$^+$ biosynthesis from Nicotinamide Riboside (NR) and from recycling after ARTD1 consumption of NAD$^+$ releasing Nicotinamide (NAM). NAM is subsequently phosphorylated by Nicotinamide Phosphoribosyl Transferase (NAMPT), an enzyme selectively inhibited by FK866. (B and C) Global NAD$^+$ (B) and global ATP (C) measurement in LN248/MPG cells after 24hr of treatment with media or FK866 (10nM). The data shown is the average of 3 independent experiments +/− SD and are reported as percentage of the untreated cells; (B)*p<0.05. (D) Seahorse measurement of the OCR metabolic profile was performed in LN428/MPG cells treated with either media control or FK866 (10nM) for 24hr. Shown is the mean of 4 independent experiments +/− SD (**p<0.01). (E) Seahorse measurement of the ECAR metabolic profile was performed as above. Shown is the mean of 2 independent experiments +/− SD. (F) Global NAD$^+$ level in LN428/MPG cells after either media, NR (1mM) or FK866 (10nM) with or without NR (1mM) as a 24hr pre-treatment. Cells treated by MNNG, and pretreated or not by NR, are

incubated 1hr with MNNG prior the analysis (***p<0.0005, **p<0.001). (G) Global ATP levels after 24hr treatment with either media (black bar) or NR (1mM) (dark grey bar), or NR (10mM) followed by media alone or media supplemented with MNNG (5μM, 1hr) (dark-grey, light-grey and white bars) (*p<0.05). (H) OCR metabolic profile of LN428/MPG cells treated with either media control or NR (1mM) and/or FK866 (10nM) followed by media alone or media supplement with MNNG (5μM, 1hr). Data shown is the mean of four independent experiments +/− SD (***p<0.005, **p<0.01, *p<0.05). (I) ECAR profile of LN428/MPG cells treated with either media or media supplemented with 1mM NR for 24hr followed by a 1hr treatment with MNNG. Data shown is the mean of three independent experiments +/− SD (**p<0.01, *p<0.05).

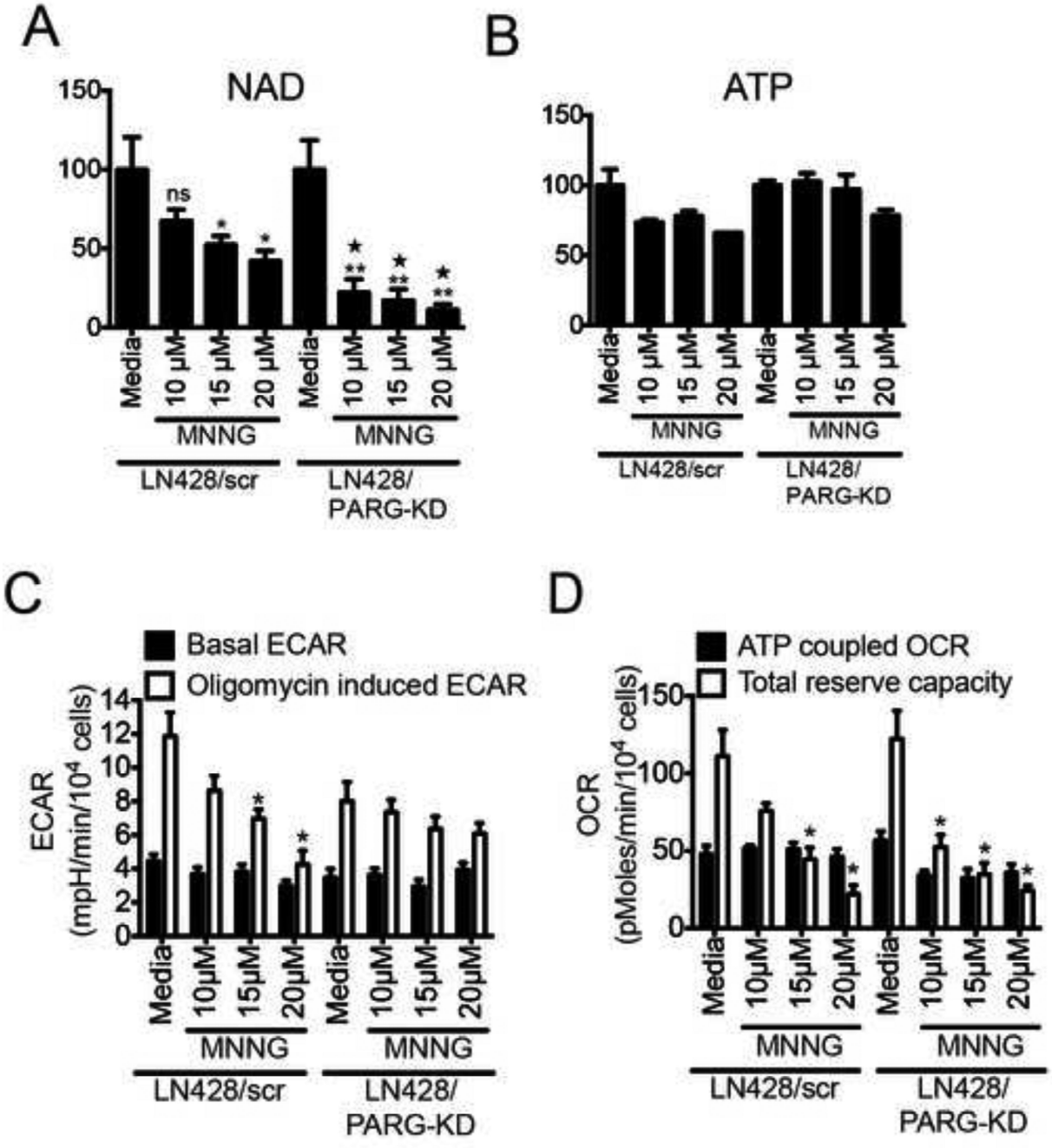

Figure 4. Absence of PARG rescues loss of ATP and glycolytic defects in LN428 cells after high dose MNNG treatment

(A and B) Global NAD^+ (A) and global ATP (B) measured in LN428/scr and LN428/PARG-KD cells after 1hr exposure to increasing doses of MNNG. Shown is the mean of 3 independent experiments (ns, non significant; *p<0.04 compared to media treated LN428/scr cells; **p<0,01 compared to media treated LN428/PARG-KD cells; ⁎p<0.005 compared to each respective dose of MNNG in LN428/scr cells). (C and D) Seahorse measurement of ECAR metabolic profile (C) and OCR metabolic profile (D) of LN428/scr

or LN428/PARG-KD cells treated with either media or MNNG (1hr) at 10μM, 15μM and 20μM. Shown is the mean of 3 independent experiments +/− SD (*p<0,05).

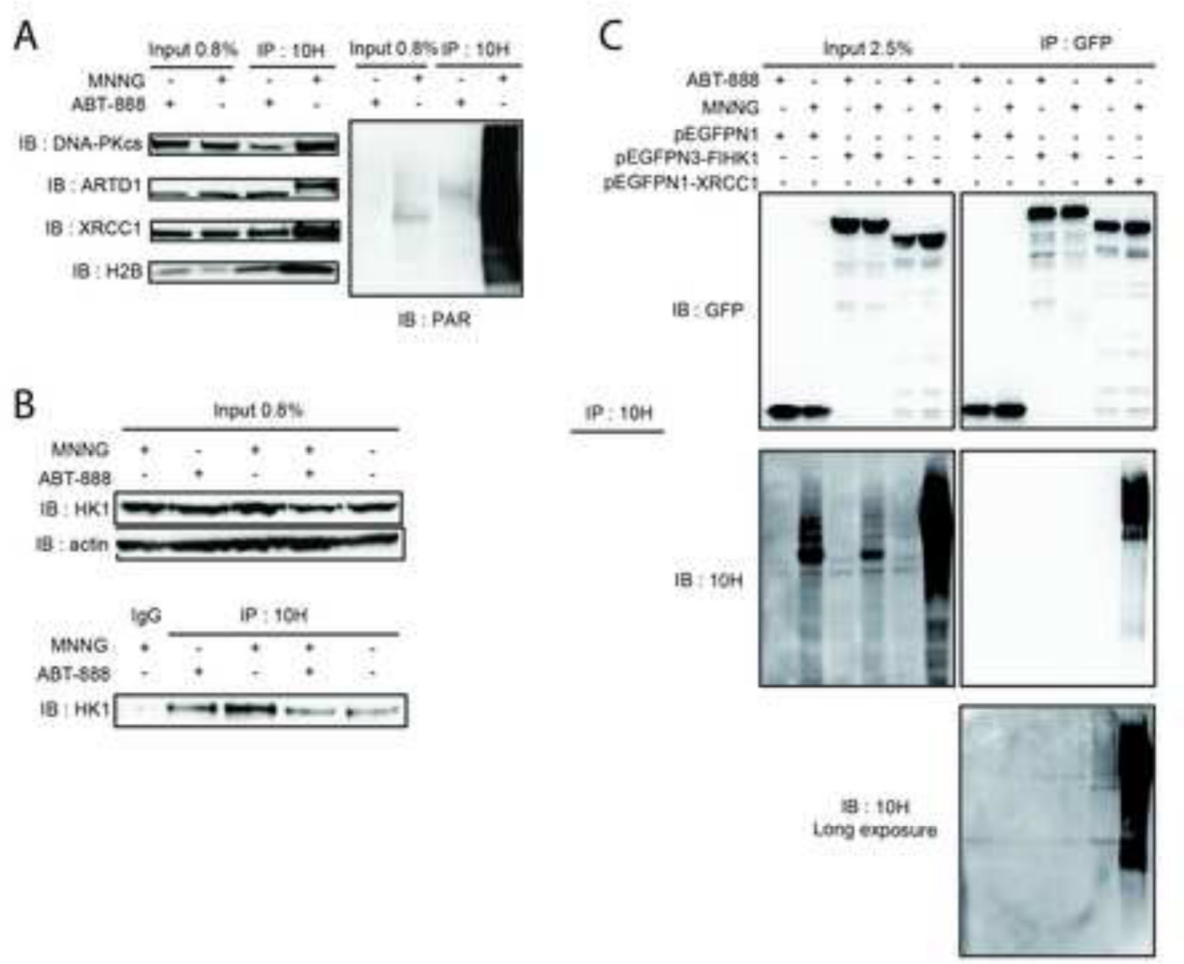

Figure 5. Affinity-purification and analysis of PAR-containing complexes

(A) Validation by IP/immunoblot of DNA-PKcs, ARTD1, XRCC1 and H2B identified in the mass spectrometry analysis. Left panel is IP with the anti-PAR Ab 10H and immunoblot with the indicated antibodies; right panel is immunoblot for PAR after IP with the anti-PAR (10H) Ab. (B) Validation by IP/immunoblot of HK1 enzyme identified in the mass spectrometry analysis as described in (A). (C) Upper panel is the GFP immunoblot on inputs and IP samples after pull-down of GFP-tagged proteins with GFP-Trap. Cells are treated either with the ARTD1 inhibitor ABT-888 (10μM; 30min) or with MNNG (5μM; 5min). Lower panel is PAR immunoblot on inputs and IPs samples. PAR immunoblot on IPs samples is shown as short and long exposures.

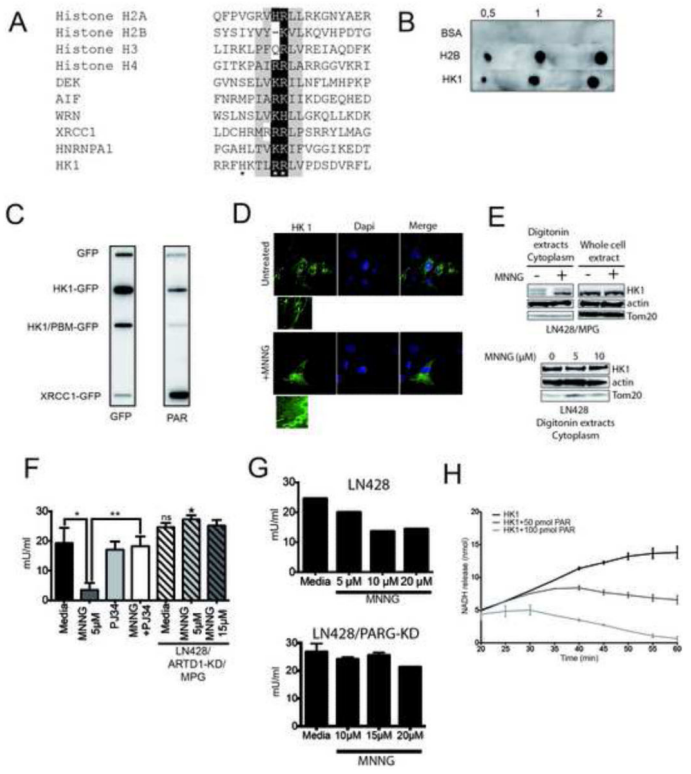

Figure 6. MNNG-mediated ARTD1 activation leads to hexokinase 1 release from the mitochondria and loss of activity

(A) Alignment of the PAR Binding domains (PBM) of histone H2A, H2B, H3, H4, DEK, AIF, WRN, XRCC1, HNRNPA1 and HK1 with the consensus PBM identified previously (Gagne et al., 2008; Pleschke et al., 2000). *indicates the amino acids in the putative PBM of HK1 mutated to alanine, A. (B) PAR dot blot performed with 0.5, 1 or 2µg BSA, histone H2B or HK1, as indicated. Shown is a one experiment among 4 performed independently. (C) PAR overlay performed by slot blot. Each protein was expressed in LN428 cells as a fusion with EGFP and isolated using GFP-Trap. The isolated proteins were bound to the membrane and incubated either with a GFP antibody (left panel) or PAR (right panel) followed by incubation with the anti-PAR (10H) antibody. (D) Immuno-detection by immunofluorescence of EGFP-tagged HK1 in LN428/MPG cells treated for 1hr with media or MNNG (5µM). (E) HK1 is released from the mitochondria, into the cytoplasm, after MNNG treatment. Immunoblot of endogenous HK1 in LN428/MPG cytosolic extracts (upper panel). Lower panel is the cytosolic extracts of LN428 cells performed after 1hr treatment with 0, 5 or 10µM MNNG. Actin is shown as a loading control and Tom20 as a control to demonstrate the absence of mitochondrial proteins. (F and G) Specific HK1-acitivity measurement in LN428/MPG (plain bars) and LN428/ARTD1-KD/MPG cells (hatched bars) (F) or LN428 (upper panel) and LN428/PARG-KD cells (lower panel) (G). LN428/MPG cells are pre-treated (1hr) with either media (black bar) or PJ34 (2µM) (light-grey bar) prior to MNNG treatment (dark-grey and white bars). Shown is the mean of 3 independent experiments +/− SD (**p<0.005, *p<0.05). LN428/ARTD1-KD/MPG cells are treated (1hr) with MNNG (5µM, hatched light-grey bar and 15µM, hatched dark-grey bar) (ns: non significant compared to LN428/MPG cells untreated, *p<0,05 compared to MNNG

treated LN428/MPG cells). LN428 and LN428/PARG-KD cells were treated with 5μM, 10μM and 20μM MNNG (1hr). (H) PAR binding leads to HK1 activity decrease *in vitro*. HK1 activity is measured *in vitro* 20min after incubation of 0.25μg of HK1 with *in vitro* synthesized PAR (50pmol or 100pmol), using an HK1 colorimetric assay. Data shown is the mean of two independent experiments +/− SD.